Environ. Sci. Technol. **2006**, *40,* 3586−3594

The Global Atmospheric Environment for the Next Generation

F. DENTENER,[*,†] D. STEVENSON,[‡] K. ELLINGSEN,[§] T. VAN NOIJE,[‖] M. SCHULTZ,[¶] M. AMANN,[⊥] C. ATHERTON,[×] N. BELL,[▽] D. BERGMANN,[×] I. BEY,[○] L. BOUWMAN,[#] T. BUTLER,[+] J. COFALA,[⊥] B. COLLINS,[●] J. DREVET,[○] R. DOHERTY,[‡] B. EICKHOUT,[#] H. ESKES,[‖] A. FIORE,[∞] M. GAUSS,[§] D. HAUGLUSTAINE,[◇] L. HOROWITZ,[∞] I. S. A. ISAKSEN,[§] B. JOSSE,[★] M. LAWRENCE,[+] M. KROL,[†] J. F. LAMARQUE,[◇] V. MONTANARO,[@] J. F. MÜLLER,[◆] V. H. PEUCH,[★] G. PITARI,[@] J. PYLE,[£] S. RAST,[¶] J. RODRIGUEZ,[°,¢] M. SANDERSON,[●] N. H. SAVAGE,[£] D. SHINDELL,[▽] S. STRAHAN,[△] S. SZOPA,[◇] K. SUDO,[⊗] R. VAN DINGENEN,[†] O. WILD,[⊗] AND G. ZENG[£]

Joint Research Centre, Institute for Environment and Sustainability, via E. Fermi 1, I-21020, Ispra, Italy, School of Geosciences, University of Edinburgh, Edinburgh, United Kingdom, Department of Geosciences, University of Oslo, Oslo, Norway, Royal Netherlands Meteorological Institute (KNMI), De Bilt, The Netherlands, IIASA, International Institute for Applied Systems Analysis, Laxenburg, Austria, Netherlands Environmental Assessment Agency (RIVM/MNP), Bilthoven, The Netherlands, Frontier Research Center for Global Change, JAMSTEC, Yokohama, Japan, Swiss Federal Institute of Technology (EPFL), Lausanne, Switzerland, NASA-Goddard Institute for Space Studies, New York, Goddard Earth Science & Technology Center (GEST), Baltimore, Maryland, Belgian Institute for Space Aeronomy, Brussels, Belgium, Lawrence Livermore National Laboratory, Atmospheric Science Division, Livermore, California, CEA/CNRS, Laboratoire des Sciences du Climat et de l'Environnement, Gif-sur-Yvette, France, Max Planck Institute for Chemistry, Mainz, Germany, Meteo-France, CNRM/GMGEC/CATS, Toulouse, France, NOAA GFDL, Princeton, New Jersey, National Center of Atmospheric Research, Atmospheric Chemistry Division, Boulder, Colorado,Max Planck Institute for Meteorology, Hamburg, Germany, Centre of Atmospheric Science, University of Cambridge, Cambridge, United Kingdom, Met Office, Exeter, United Kingdom, Dipartimento di Fisica, Università L'Aquila, L'Aquila, Italy, and University of Miami, Coral Gables, Florida, NASA-Goddard Space Flight Center, Baltimore, Maryland

* Corresponding author phone: +390332786392; fax +390332786291; e-mail frank.dentener@jrc.it.
† Joint Research Centre, Institute for Environment and Sustainability.
‡ University of Edinburgh.
§ University of Oslo.
‖ Royal Netherlands Meteorological Institute (KNMI).
⊥ IIASA, International Institute for Applied Systems Analysis.
\# Netherlands Environmental Assessment Agency (RIVM/MNP).
⊗ Frontier Research Center for Global Change, JAMSTEC.
○ Swiss Federal Institute of Technology (EPFL).
▽ NASA-Goddard Institute for Space Studies.
△ Goddard Earth Science & Technology Center (GEST).
◆ Belgian Institute for Space Aeronomy.
× Lawrence Livermore National Laboratory.
◇ CEA/CNRS.
\+ Max Planck Institute for Chemistry.
★ Meteo-France, CNRM/GMGEC/CATS.
∞ NOAA GFDL.
◇ National Center of Atmospheric Research.
¶ Max Planck Institute for Meteorology.
£ University of Cambridge.
● Met Office, Exeter.
@ Università L'Aquila.
° University of Miami.
¢ NASA-Goddard Space Flight Center.

Air quality, ecosystem exposure to nitrogen deposition, and climate change are intimately coupled problems: we assess changes in the global atmospheric environment between 2000 and 2030 using 26 state-of-the-art global atmospheric chemistry models and three different emissions scenarios. The first (CLE) scenario reflects implementation of current air quality legislation around the world, while the second (MFR) represents a more optimistic case in which all currently feasible technologies are applied to achieve maximum emission reductions. We contrast these scenarios with the more pessimistic IPCC SRES A2 scenario. Ensemble simulations for the year 2000 are consistent among models and show a reasonable agreement with surface ozone, wet deposition, and NO_2 satellite observations. Large parts of the world are currently exposed to high ozone concentrations and high deposition of nitrogen to ecosystems. By 2030, global surface ozone is calculated to increase globally by 1.5 ± 1.2 ppb (CLE) and 4.3 ± 2.2 ppb (A2), using the ensemble mean model results and associated ±1 σ standard deviations. Only the progressive MFR scenario will reduce ozone, by −2.3 ± 1.1 ppb. Climate change is expected to modify surface ozone by −0.8 ± 0.6 ppb, with larger decreases over sea than over land. Radiative forcing by ozone increases by 63 ± 15 and 155 ± 37 mW m^{-2} for CLE and A2, respectively, and decreases by −45 ± 15 mW m^{-2} for MFR. We compute that at present 10.1% of the global natural terrestrial ecosystems are exposed to nitrogen deposition above a critical load of 1 g N m^{-2} yr^{-1}. These percentages increase by 2030 to 15.8% (CLE), 10.5% (MFR), and 25% (A2). This study shows the importance of enforcing current worldwide air quality legislation and the major benefits of going further. Nonattainment of these air quality policy objectives, such as expressed by the SRES-A2 scenario, would further degrade the global atmospheric environment.

Introduction

Emissions of reactive trace gases, generated in the burning of fossil- and biofuels and volatilized from agricultural processes, cause a number of environmental problems. Ozone (O_3) forms from the photochemical oxidation of methane (CH_4), carbon monoxide (CO), and volatile organic components (NMVOC) in the presence of nitrogen oxides (NO_x=NO+NO_2). O_3 is an important greenhouse gas and is also toxic to humans, animals, and plants. The IPCC Third Assessment Report (*1*) recognized that conventional air pollutant emissions affect climate directly (through O_3 and aerosol production) and indirectly through their influence on the CH_4 lifetime. An evaluation of the high-emissions IPCC SRES A2 emissions scenario showed global mean surface O_3 increases of about 5 ppb by 2030 and 20 ppb by 2100 (*2*). Enhanced emissions of sulfur dioxide (SO_2), NO_x, and ammonia (NH_3) lead to increased long-range transport and

10.1021/es0523845 CCC: $33.50
© 2006 American Chemical Society
Published on Web 04/19/2006

TABLE 1. Overview of Simulations, Prescribed Methane Volume Mixing Ratios, and Global Anthropogenic Emissions of CO, NMVOC, NO_x, SO_2, and NH_3[a]

simulation	meteorology	description	CH_4 [ppb]	CO	NMVOC	NO_x (NO_2)	SO_2	NH_3
S1-B2000	CTM 2000 GCM SSTs 1990s	baseline	1760	977.0	147.1	124.8	111.1	64.8
S2-CLE/CLEc	CTM 2000 GCM SSTs 1990s	IIASA CLE 2030, current legislation scenario	2088	904.1	145.5	141.1	117.6	84.8
S3-MFR	CTM 2000 GCM SSTs 1990s	IIASA MFR 2030, maximum feasible reduction scenario	1760	728.7	104.4	76.0	35.8	84.8
S4-A2	CTM 2000 GCM SSTs 1990s	SRES A2 2030, the most 'pessimistic' IPCC SRES scenario	2163	1268.2	206.7	206.7	202.3	89.2
S5c-CLE2030c	only GCM SSTs 2030s	IIASA CLE 2030 + climate change	2012	904.1	145.5	141.1	117.6	84.8

[a] Emissions in Tg full molecular weight/year. Additional information is found in the Supporting Information

deposition of nitrogen and sulfur, damaging eutrophication and acidification of ecosystems and loss of biodiversity (*3*, *4*).

In this work we evaluate the effect of changing emissions and climate on ozone air quality, radiative forcing, and nitrogen deposition to ecosystems for the year 2030. We use a recently developed set of emission scenarios (*5*) for CH_4, NO_x, NH_3, CO, SO_2, and NMVOC, which differ substantially from the previous SRES scenarios (*6*). In the past few years increasing air pollution in developing countries has become a public concern ((*5*) and references therein). Consequently, many of the major rapidly developing countries in Asia and Latin America have issued legislation requiring emission controls. Upon implementation, these regulations will significantly cap the air pollution emissions at the regional and global scales. This is the basis of our CLE (Current LEgislation) scenario. Further, we evaluate the effects of the emissions of a MFR (maximum technologically feasible reduction) scenario and contrast it with the pessimistic SRES A2 scenario. These emission scenarios were used internationally, by 26 established global atmospheric chemistry-transport models (CTMs) driven by analyzed meteorological fields or general circulation models (GCMs). Although some models share subcomponents, the ensemble of model results is sufficiently broad to estimate uncertainties resulting from the various assumptions in the models. The models performed baseline (year 2000) and 2030 scenarios, all using a fixed meteorology relevant for the year 2000; a subset of models repeated the 2030 CLE scenario but with a changed climate. In this paper we give an integrative overview of the findings; other publications (*7*−*10*) present more detailed results from this large model exercise.

Methods

Up to five simulations were performed by each model (Table 1): B2000 evaluated the reference year 2000, while CLE, MFR, and A2 assessed the year 2030. We show in the Supporting Information the importance of emission controls in the CLE and MFR scenario as compared to SRES A2. To avoid excessive equilibration times of CH_4 we prescribed global CH_4 volume mixing ratios, using consistent values from earlier transient simulations for 1990−2030 described in refs *5* and *11*. GCMs performed 5−10 years of simulations, using a climate appropriate for the time period 1995−2004. To evaluate the impacts of climate change, an additional simulation (CLE2030c) was computed by 10 of the GCM-driven models, using a climate appropriate for 2030. Most modelers applied the IS92a climate scenario associated with a global mean surface warming of about 0.7 K between 2000 and 2030. In the Supporting Information we present the 26 participating models, including characteristics of their resolution, chemistry and transport parametrizations, and key publications. Compared to earlier IPCC modeling exercises (*2*, *12*) twice as many models participated in this study; model complexity (inclusion of NMVOC chemistry) and resolutions have increased: half of the models had horizontal resolutions of 2°−3° or better, and most of the other models had resolutions around 4°−5°. In the following discussion we focus on the unweighted ensemble mean of the model results, expressing the variability of the results as the $\pm 1\ \sigma$ standard deviation. We note that the $\pm 1\ \sigma$ interval should be interpreted as a lower bound for model uncertainty, which contains additional unquantified processes. In general, we found relatively small (<10%) differences between mean and median model results.

Results

Surface Ozone. In Figure 1a−d we display the ensemble mean annual average surface O_3 for B2000 and O_3 differences for CLE, MFR, and A2 in 2030. Figure 1a shows that calculated annual average ensemble mean surface O_3 ranges from 40 to 50 ppb over large parts of North America, Southern Europe, and Asia. Background values are 15−25 ppb in large parts of the Southern Hemisphere (SH). Average surface mixing ratios are 33.7 ± 3.8 ppb and 23.7 ± 3.7 ppb (Table 2), for the Northern Hemisphere (NH) and SH, respectively. In Figure 1a we also give averaged measurements for the year 2000. Our analysis reveals that our mean model results are within 5 ppb of the measurements in the United States, China, and Central Europe and may overestimate the measured annual average by 10−15 ppb in Africa, India, and the Mediterranean. The reason for this overestimate is not clear but may be related to overestimates of NO_x or NMVOC emissions in these regions. Also, the regional representativeness of the sparse measurements may be poor, and measurement precision may also play a role. These issues are currently under further investigation.

The CLE scenario (Figure 1b, Table 2) would approximately stabilize O_3 in 2030 at 2000 levels in parts of North America, Europe, and Asia. However, O_3 may increase by more than 10 ppb in areas anticipated to experience large emission increases in the transport and power generation sectors (e.g. India). Background O_3 increases by 2−4 ppb in the tropical and mid-latitude NH related to worldwide changes in CH_4, NO_x, CO, and NMVOC emissions. The increases are most consistently predicted in Asia, whereas the ensemble predictions have large standard deviations in North and South America, Southern Africa, and the Middle East. A cleaner future is possible, if all currently available technologies are used to abate O_3 precursor emissions. In this MFR case (Figure 1c; Table 2) O_3 decreases by 5−10 ppb in the most polluted regions. The models are consistent in their prediction of surface ozone reductions with relative standard deviations of 30−40%. Finally, consistent with previous studies (*2*), in the A2 scenario (Figure 1d), annual average surface O_3 increases by 4 ppb worldwide and by 5−15 ppb in Latin America, Africa, and Asia.

How is climate change expected to influence these O_3 changes? The average results from 10 models for the CLE2030c scenario shown in Figure 1e indicate that climate change may reduce surface O_3 by 1−2 ppb over the oceans and by 0.5−1 ppb over the continents, although some regions, such as the Eastern United States, may experience increases.

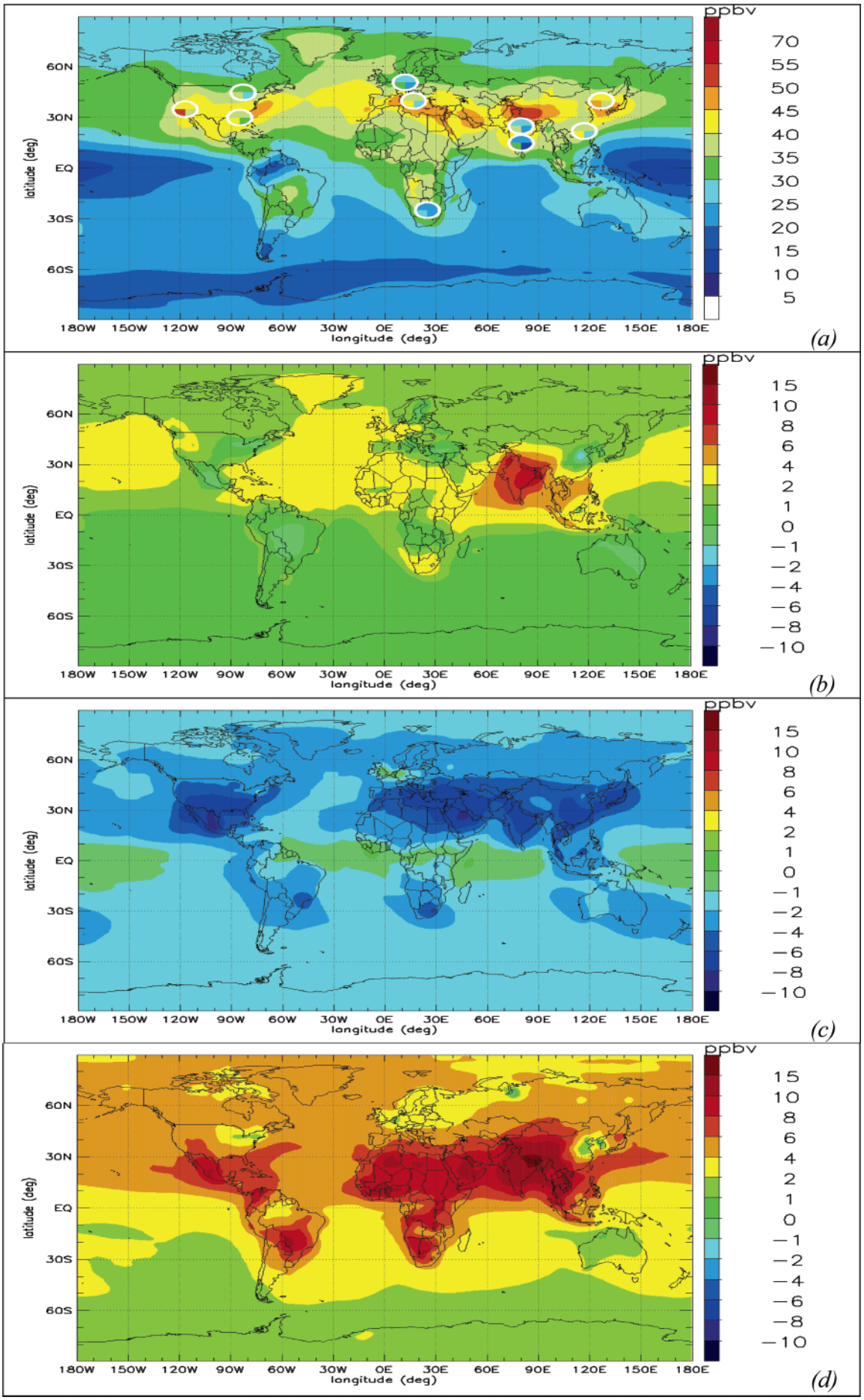
ppbv
70
55
50
45
40
35
30
25
20
15
10
5
60N
30N
EQ
30S
60S
latitude (deg)
180W 150W 120W 90W 60W 30W 0E 30E 60E 90E 120E 150E 180E
longitude (deg)
(a)
ppbv
15
10
8
6
4
2
1
0
−1
−2
−4
−6
−8
−10
(b)
(c)
(d)

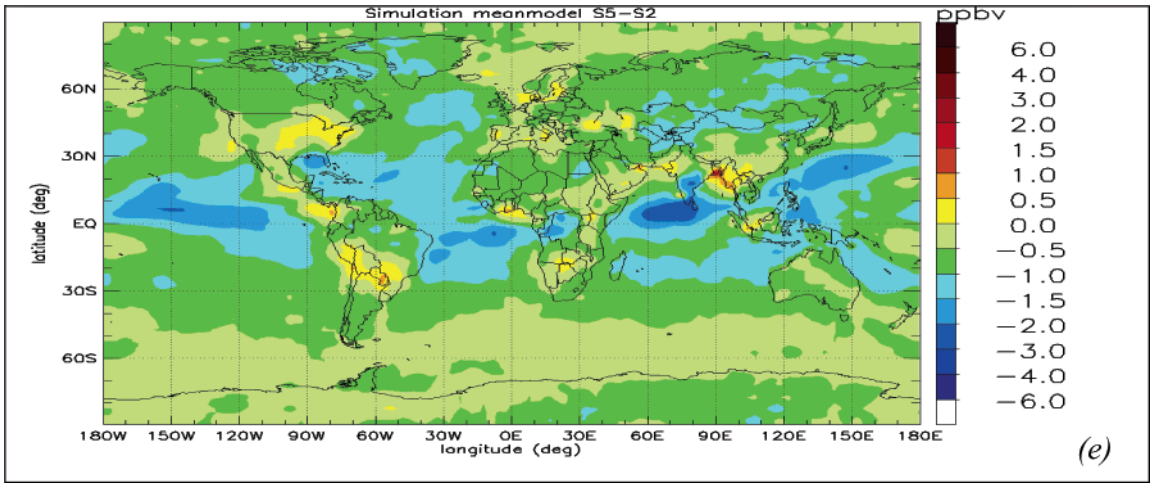

FIGURE 1. Ensemble mean (a) ozone in the year 2000 and ozone differences between scenarios (b) CLE, (c) MFR, (d) A2 with 2000, and (e) impact of climate change, comparing CLEc and CLE. Regionally averaged measurements (upper: mean, lower left mean + 1σ, lower right mean − 1σ) are given in circles. Measurements are taken from taken from the WMO-GAW World Data Centre for surface ozone, EMEP/AIRBASE in Europe, and CASTNet in the United States. Measurements for India, China, and Africa are from various scientific studies (*19*−*22*).

TABLE 2: Area Weighted Regional and Global Annual Mean Surface O_3 [ppb], SOMO35 [ppb days], and Tropospheric O_3 Column [DU] in 2000 and Increases for Various Scenarios at Selected Regions[a]

region		O_3 2000 n = 26/17/26	ΔO_3 CLE2030-B2000 n = 26/14/26	ΔO_3 MFR2030-B2000 n = 21/14/21	ΔO_3 A2_2030-B2000 n = 21/14/21	ΔO_3 CLE2030c-CLE2030 n = 10/-/10
United States	O_3 surf	38.7 ± 4.9	1.3 ± 2.4	**−4.9 ± 1.8**	**4.8 ±4.5**	−0.4 ± 1.2
	SOMO35	4145 ± 1378	**583 ± 280**	**−1788 ± 525**	**1911 ± 797**	nd
	column	37.0 ± 5.0	**2.1 ± 0.6**	**−2.5 ± 0.6**	**5.2 ± 1.2**	0.1 ± 0.7
South America	O_3 surf	27.9 ± 4.7	0.5 ± 2.0	**−2.4 ± 2.3**	**5.7 ± 2.7**	−0.5 ± 0.8
	SOMO35	1681 ± 865	**140 ± 74**	**−231 ± 106**	**1247 ± 597**	nd
	column	35.2 ± 5.5	**1.3 ± 0.4**	**−1.2 ± 0.3**	**4.9 ± 1.1**	−0.2 ± 0.4
Southern Africa	O_3 surf	34.8 ± 5.0	1.4 ± 3.9	**−2.5 ± 4.5**	**7.0 ± 4.2**	−0.4 ± 0.7
	SOMO35	3207 ± 1304	**553 ± 190**	**−332 ± 126**	**2084 ± 666**	nd
	column	35.2 ± 5.5	**1.7 ± 0.4**	**−1.1 ± 0.3**	**5.7 ± 1.3**	0.1 ± 0.4
OECD Europe	O_3 surf	36.6 ± 4.2	**1.8 ± 1.5**	**−2.8 ± 1.1**	**3.9 ±q 3.8**	−0.4 ± 0.7
	SOMO35	3056 ± 1084	**384 ± 335**	**−1071 ± 2 92**	**1417 ± 823**	nd
	column	37.3 ± 4.9	**2.0 ± 0.6**	**−2.1 ± 0.5**	**4.7 ± 1.2**	−0.1 ± 0.4
Middle East	O_3 surf	43.5 ± 6.4	**1.7 ± 2.4**	**−6.6 ± 2.2**	**8.7 ± 6.0**	−0.6 ± 0.9
	SOMO35	5388 ± 1917	**766 ±401**	**−2195 ± 668**	**3692 ± 1523**	nd
	column	42.4 ± 5.6	**2.68 ± 0.7**	**−2.7 ± 0.7**	**7.1 ± 1.5**	0.0 ± 0.7
South Asia	O_3 surf	45.0 ± 6.9	**7.2 ± 1.9**	**−5.9 ± 1.6**	**11.8 ± 4.3**	−0.7 ± 0.9
	SOMO35	6093 ± 2266	**3094 ± 791**	**−1976 ± 560**	**4914 ± 1435**	nd
	column	42.7 ± 6.0	**4.0 ± 0.8**	**−2.5 ± 0.6**	**7.9 ± 1.6**	−0.2 ± 0.6
South East Asia	O_3 surf	31.5 ± 4.4	**3.8 ± 0.7**	**−3.6 ± 0.5**	**7.7 ± 1.8**	−0.6 ± 1.0
	SOMO35	2096 ± 937	**945 ± 329**	**−703 ± 276**	**2222 ± 563**	nd
	column	32.3 ± 5.6	**2.9 ± 0.7**	**−1.8 ± 0.5**	**5.6 ± 1.5**	−0.3 ± 0.6
Northern Hemisphere	O_3 surf	33.7 ± 3.8	**2.3 ± 0.5**	**−2.9 ± 0.6**	**5.9 ± 2.1**	**−0.8 ± 0.7**
	SOMO35	2336 ± 950	**615 ± 254**	**−786 ± 208**	**1738 ± 704**	nd
	column	35.8 ± 5.4	**2.2 ± 0.6**	**−1.9 ± 0.5**	**5.3 ± 1.4**	−0.2 ± 0.7
Southern Hemisphere	O_3 surf	23.7 ± 3.7	**0.6 ± 2.1**	**−1.7 ± 2.3**	**2.7 ± 2.6**	**−0.7 ± 0.6**
	SOMO35	486 ± 330	**111 ± 85**	**−79 ± 55**	**394 ± 229**	nd
	column	29.4 ± 5.1	**1.2 ± 0.4**	**−0.9 ± 0.3**	**3.4 ± 1.0**	−0.2 ± 0.6
World	O_3 surf	28.7 ± 3.6	**1.5 ± 1.23**	**−2.3 ± 1.1**	**4.3 ± 2.2**	**-0.8 ± 0.6**
	SOMO35	1411 ± 608	**63 ± 160**	**−433 ± 118**	**1066 ± 426**	nd
	column	32.6 ± 5.3	**1.7 ± 0.5**	**−1.4 ± 0.4**	**4.3 ± 1.2**	−0.2 ± 0.6

[a] Regions are defined according to IMAGE2.2 (http://arch.rivm.nl/image/). Standard deviations are calculated from 'n' models (not all models submitted data for SOMO35). The ±1σ standard deviations reflect the variation of the regional average of the ensemble members. Ozone changes larger than 1σ are indicated in bold.

Climate-driven increases in temperature and water vapor tend to decrease surface O_3 in the cleanest regions but tend to increase O_3 in more polluted areas. A larger influx of stratospheric O_3 into the troposphere leads to a general increase of free tropospheric O_3. Note that many feedbacks, e.g. from natural emission changes, were generally not included in the models. We further note the large variability in the calculated climate impacts [Table 2].

What is the effect on ozone air quality? Several regulatory O_3 air quality limits, with threshold values of 60−80 ppb, are currently employed in Europe, the United States, and Japan. On the basis of epidemiological studies of O_3 related health effects (*13*), the World Health Organization (WHO) recommends use of the SOMO35 air quality index (ppb days), which is defined as the daily maximum of an 8-h running average ozone volume mixing ratio ($M8hO_3$, in ppb) after subtracting a 35 ppb "background" level:

$$\sum_{\text{day}=1}^{\text{day}=365/366} [\text{MAX}[(M8hO_3 - 35),0] \qquad (1)$$

In contrast to other air quality indices, SOMO35 considers O_3 toxicity to have a lower threshold and is more suited to

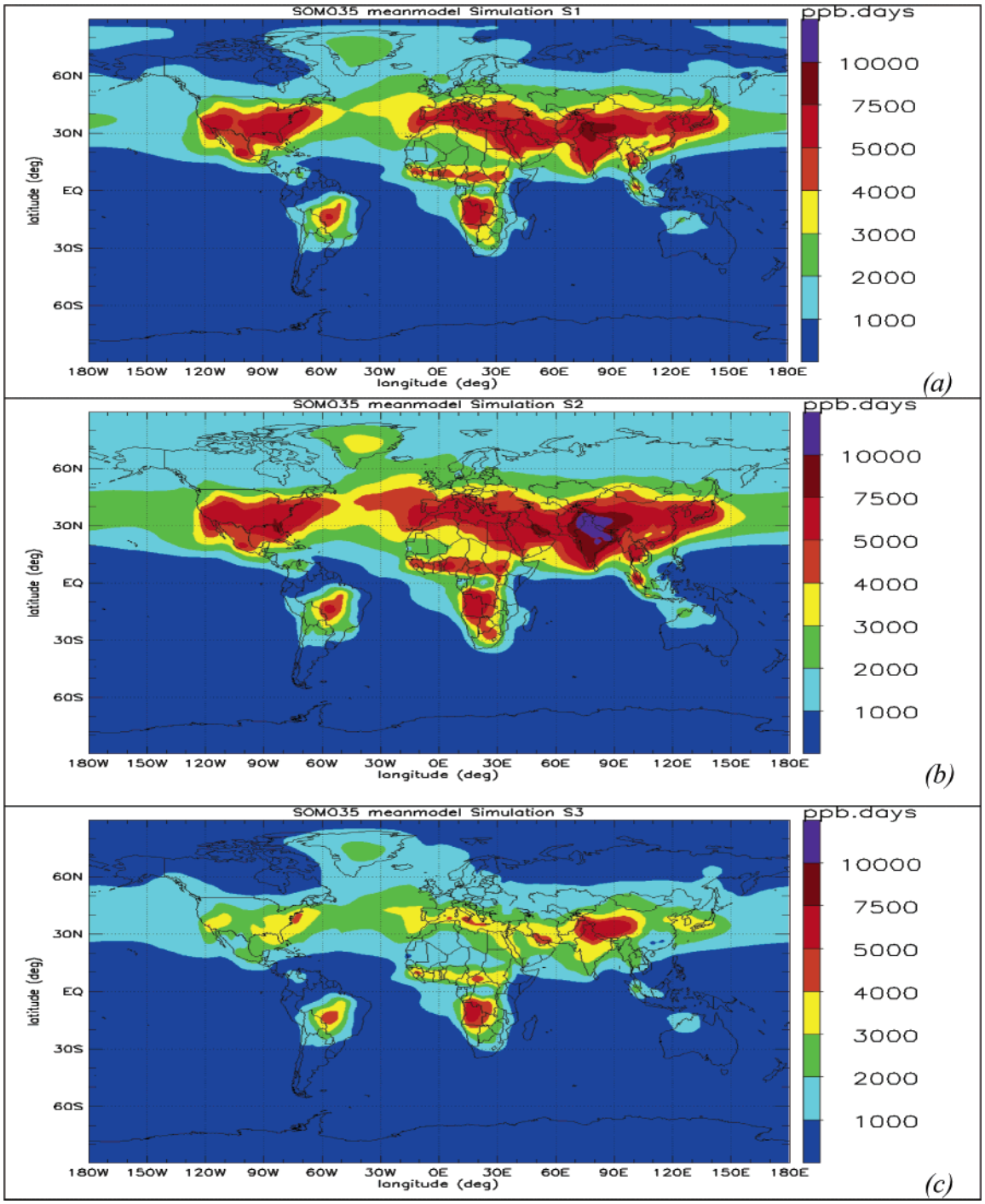

FIGURE 2. Ensemble mean SOMO35 [ppb days] (a) in the year 2000; (b) 2030 CLE; and (c) 2030 MFR.

assess the effect of large scale changes of ozone background concentrations calculated with global models. Note that SOMO35 is also rather similar to the widely used metric, AOT40, which evaluates the accumulated exposure of vegetation to ozone levels above 40 ppb.

Figure 2a−c gives SOMO35 for B2000, CLE, and MFR, and in Table 2 we give a regional analysis of SOMO35. No limit values have been established for SOMO35, but a threshold of ~3000 ppb days is consistent with air quality limits currently in use in North America and Europe (*8*). According to our model calculations this threshold (yellow and red colors) is exceeded in large parts of the world in the year 2000, most notably in the United States, the Middle East, and South Asia. In the CLE scenario this situation is aggravated especially in South Asia due to a large growth of emissions from the transport sector. Our model results indicate that the more polluting SRES A2 scenario would compromise attainment of any existing air quality standard in most industrialized parts of the world by 2030. Only the MFR scenario predicts that ozone in all regions will be at or below the current air quality standards. The large scale regional and annual averaged ozone and SOMO35 are highly correlated (r=0.99).

Radiative Forcing from Tropospheric Ozone. In Table 2 we present regional changes in tropospheric column ozone [Dobson units; DU] resulting from the emission scenarios. The current global average tropospheric ozone column is calculated to be 33 ± 5 DU in close agreement with IPCC(1), with regional averaged values in the Northern Hemisphere ranging from 32 to 42 DU. Compared to the simulation B2000,

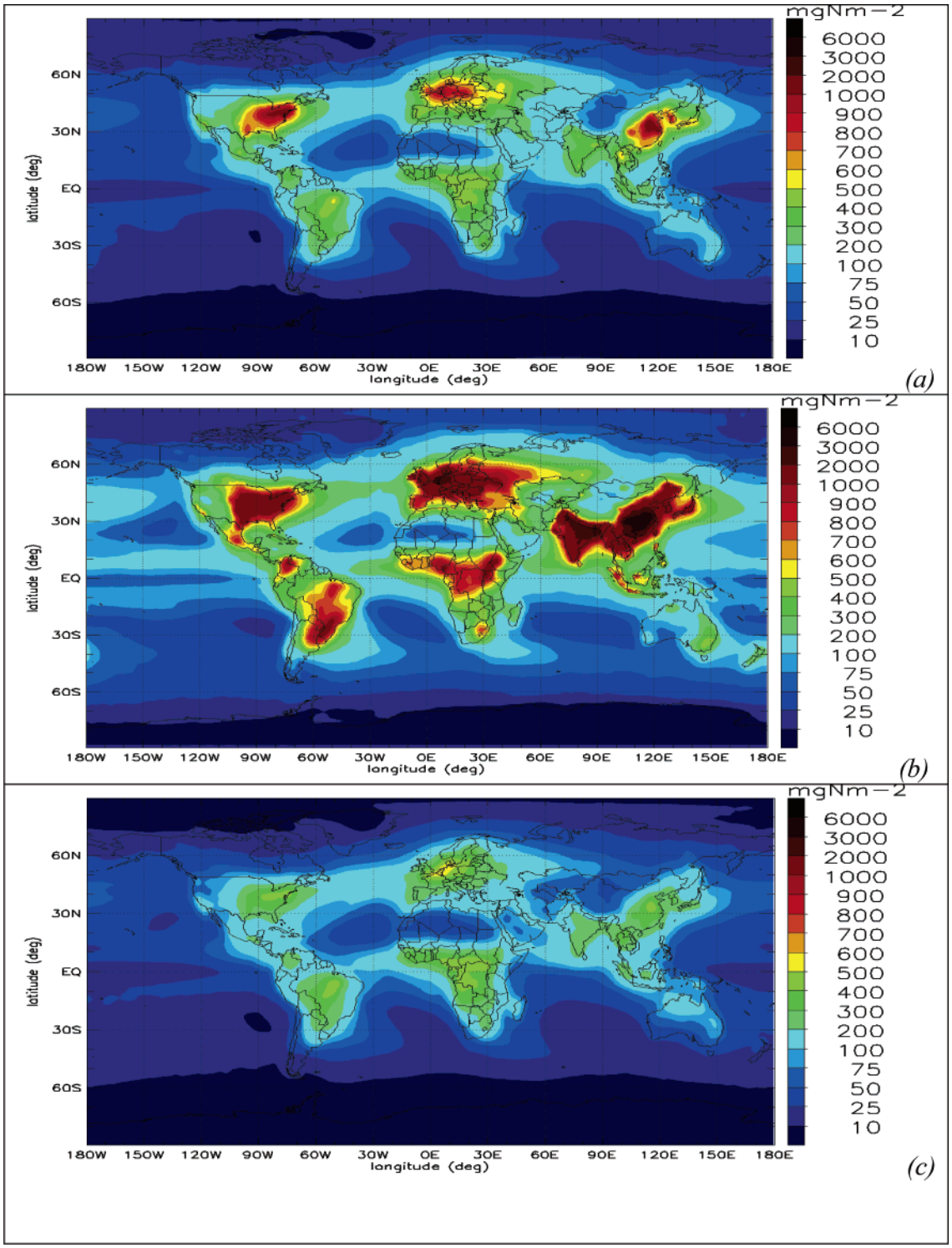

FIGURE 3. Ensemble mean (a) NO_y total deposition [mg N m^{-2} yr^{-1}] in 2000, (b) total reactive nitrogen (=NO_y+NH_x) deposition [mg N m^{-2} yr^{-1}] in 2000, and (c) MFR 2030 NO_y total deposition.

the global tropospheric ozone column increases by 1.7 ± 0.5 and 4.3 ± 1.2 DU for CLE and A2 and decreases by −1.4 ± 0.4 DU for MFR. Climate change (CLE2030c-CLE2030) leaves global tropospheric ozone relatively unaffected with a change of −0.2 ± 0.6 DU. The impact of emission reductions and increases is relatively uniform for MFR and A2, whereas the CLE scenario amplifies the regional contrast in the ozone columns and hence possible climate impacts. We find global radiative forcings increments of 63 ± 15 and 155 ± 37 mW m^{-2} for CLE and A2, respectively, and reductions of −45 ± 17 mW m^{-2} for MFR (*10*). Increases in forcings can be as high as 300 mW m^{-2} in Asia. We calculate that the sum of the O_3 and CH_4 radiative forcings, in the CLE and A2 simulations, contributes 23% and 29%, respectively, to the forcings of CO_2 alone, whereas MFR would imply a small decrease of 5% (*10*).

Nitrogen Deposition. It is currently thought that 1000 mg N m^{-2} yr^{-1} is a threshold ("critical nitrogen load"), above which changes in sensitive natural ecosystems may occur (*4*, *14*). So far most studies have focused on the effects of NO_y deposition (*15*), since it is intimately associated with O_3 formation. In Figure 3a we give the calculated NO_y deposition

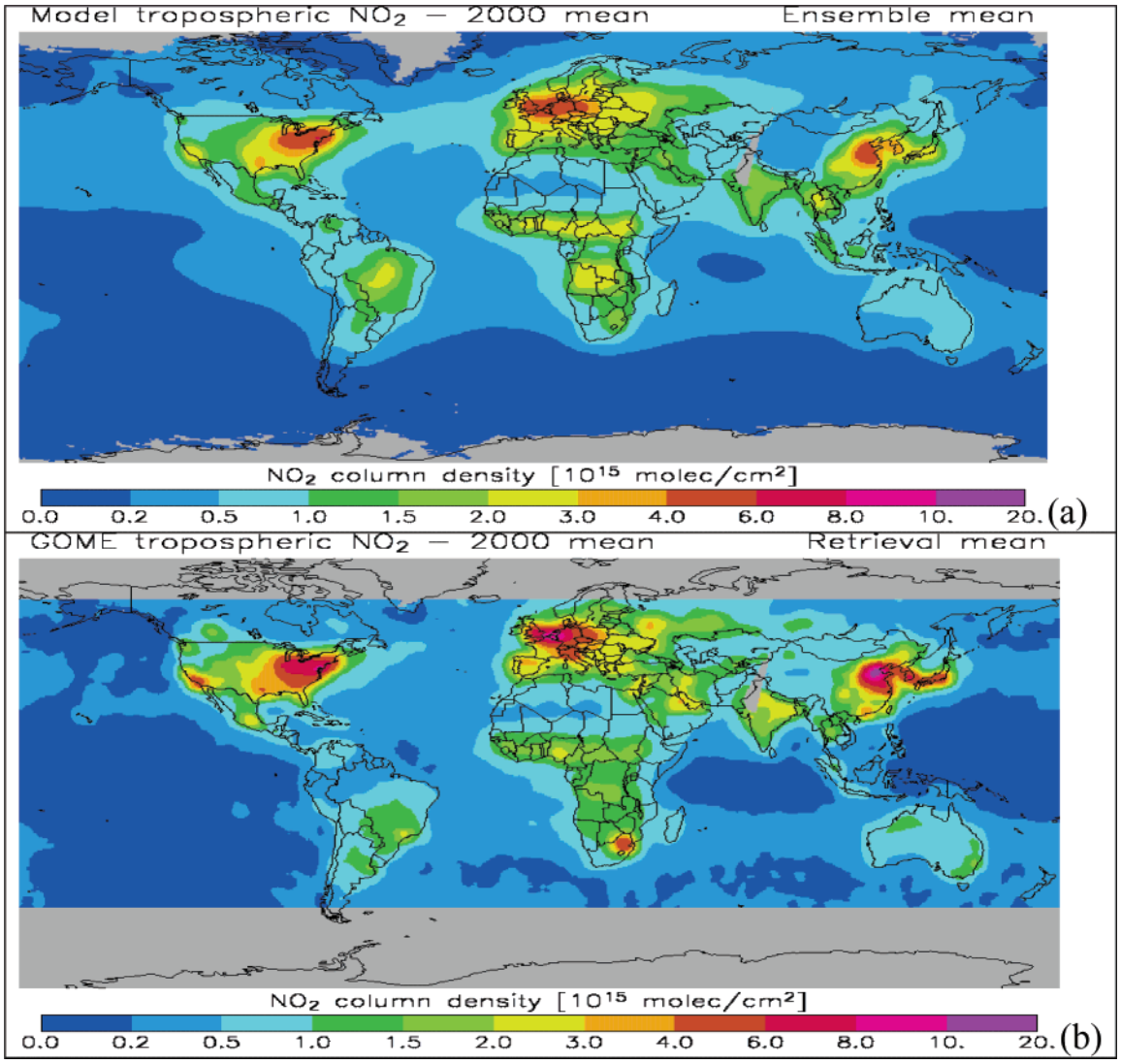

FIGURE 4. (a) Modeled and (b) GOME measured annual average NO_2 columns for the year 2000. Modeled data represent an average of 17 models, and the GOME retrieval is an average of three retrieval products. For a consistent comparison, the data in both cases have been smoothed to a horizontal resolution of 5° × 5°.

(NO_y = NO + NO_2 + NO_3 + $2N_2O_5$ + HNO_3 + particulate inorganic NO_3 and organic nitrates) in the year 2000, showing that NO_y deposition alone leads to an exceedance of this threshold in parts of the Northeast United States, Europe, and China. NH_x deposition, related to emissions from animal and food production systems, may double the deposition from NO_y. In 2000 the deposition of total reactive nitrogen (=NO_y+NH_x) exceeds 2000 mg Nm^{-2} yr^{-1} in extended parts of the world, including biodiversity hotspots (Figure 3b). To date, the consequences for biodiversity and ecosystem health have only been studied for temperate regions, but it has been suggested that increased nitrogen deposition will play an important future role in the decrease of plant diversity worldwide (*16*). A comparison of the corresponding calculated wet deposition fluxes with measurements in the United States, Europe, Southeast Asia, Africa, and South America yields agreement within a factor of 2 for 70−80% of the measurement stations. Exceptions are Asia, where the models strongly underestimate NO_y deposition by up to 60%, and South America, where almost no measurement data were found. In 2030, considering the CLE scenario NO_y deposition decreases in Europe by 30−50% (not shown), is near-constant in North America, and strongly increases in Asia by 30−100%. NH_x deposition increases almost everywhere by 50−100%, except in Europe. Our clean MFR scenario (Figure 3c), which was evaluated only for NO_y, considerably improves this situation, with NO_y deposition almost everywhere below 500 mg N m^{-2} yr^{-1}. In contrast, the A2 scenario in the year 2030 leads to extended regions exposed to NO_y deposition larger than 1000 mg N m^{-2} yr^{-1}. The CLE and A2 scenarios project further increases in nitrogen critical loads, with particularly large impacts in Asia where nitrogen emissions and deposition are forecast to increase by a factor of 1.4 (CLE) to 2 (A2). We calculate (*7*) that at present 10% of the natural terrestrial ecosystems receive nitrogen inputs above 1000 mg N m^{-2} yr^{-1}. These percentages increase by 2030 to 16% (CLE), 11% (MFR), and 25% (A2). We note that we did not determine maximum feasible emissions reductions for NH_3; instead we used in scenario S3-MFR the CLE NH_3 emissions.

Comparison with Satellite Observations of NO_2 Columns. Recent satellite observations allow us to evaluate nitrogen pollution on near global scales. For the year 2000, the GOME instrument aboard the ERS-2 satellite provides a unique opportunity to compare model calculated NO_2 columns with measurements. We sample model NO_2 columns at the satellite overpass time (10:30 LT). Daily tropospheric NO_2 column densities were calculated by 17 different models; uncertainties in the retrievals are quantified by using three different retrieval algorithms (*9*).

Low tropospheric NO_2 columns of $<1 \times 10^{15}$ molec cm^{-2} are calculated and observed by GOME in marine regions. Over the continents, three regions of dominant NO_2 pollution are found in North America, Western Europe, and China, coinciding with the regions of high emissions. These regions are also indicated in the model ensemble mean, but the averaged model maxima of $6-8 \times 10^{15}$ molec cm^{-2} underestimates the GOME observed values, which exceed 10×10^{15} molec cm^{-2}. The discrepancy between models and measurements is particularly pronounced over the rapidly developing parts of Eastern China and South Africa, indicating that the assumed NO_x emissions may be unrealistically low in these regions. In regions dominated by biomass burning, such as in Africa and South America, the models tend to overestimate the observed seasonal cycle.

We note that the discrepancy in the NO_2 column in e.g. North America and Europe does not seem consistent with the general agreement in NO_3 wet deposition. In the rapidly developing parts of China and Southern Africa, the model-satellite discrepancy indicates an underestimate of NO_x emissions, consistent with underestimates of N-deposition, but not corroborated by similar discrepancies in surface ozone. One important finding, however, is that the differences of the GOME retrievals are in many instances as large as the spread in model results, meaning that in only a few cases (i.e. in China) robust statements on underprediction of NO_x emissions can be made.

The Present and Future Atmospheric Environment. Our study evaluates how different scenarios of pollutant emissions influence present and future surface ozone air quality, climate forcing, and nitrogen deposition. Surface based and satellite observations confirm our assessment of the present-day pollution. We show that by 2030 the present worldwide legislation on air pollutant emissions is not sufficient to stabilize or reduce the current problems related to ozone and eutrophication. Moreover we note that the current lack of experience with the introduction of air pollution policies in developing countries, which may delay the actual implementation of such legislation. The SRES A2 scenario, associated with strong increases in surface ozone, radiative forcing, and deposition, offers one depiction of a world where air pollution policies are not attained. Only the introduction of stringent NO_x, CO, NMVOC, and CH_4 abatement technologies (MFR) prevents additional climate forcing by O_3 and may bring surface O_3 and eutrophication of ecosystems to more acceptable levels. Our MFR scenario, however, was constructed without considering the implementation costs of these technical measures. Further integrated analysis of the costs and benefits of reducing NH_3, NO_x, CO, NMVOC, and CH_4 emissions (*5*, *17*, *18*) in the context of climate and air pollution policies is needed to guarantee a cleaner atmospheric environment for the next generation.

Acknowledgments

This model exercise was organized under the umbrella of the EC FP6 Network of Excellence ACCENT.

Supporting Information Available

Details on the participating models and assumptions made in the emissions scenarios are presented. This material is available free of charge via the Internet at http://pubs.acs.org.

Literature Cited

(1) Prather, M.; Ehhalt, D.; Dentener, F.; Derwent, R.; Dlugokencky, E.; Holland, E.; Isaksen, I.; Katima, J.; Kirchhoff, V.; Matson, P.; Midgley, P.; Wang, M. In *Climate Change 2001, The scientific basis: Contribution of working group I to the Third assessment report of the Intergovernmental Panel on Climate*; Houghton, J. T., Ding, Y., Griggs, D. J., Noguer, M., Linden, P. J. v. d., Dai, X., Maskell, K., Johnson, C. A., Eds.; Cambridge University Press: Cambridge, United Kingdom and New York, U.S.A., 2001; p 881.

(2) Prather, M.; Gauss, M.; Berntsen, T. K.; Isaksen, I.; Sundet, J.; Bey, I.; Brasseur, G.; Dentener, F.; Derwent, R.; Stevenson, D. S.; Grenfell, L.; Hauglustaine, D.; Horowitz, L. W.; Jacob, D.; Mickley, L. J.; Lawrence, M. G.; Kuhlman, R. v.; Muller, J.-F.; Pitari, G.; Rogers, H.; Johnson, M.; Pyle, J. A.; Law, K. S.; Weele, M. v.; Wild, O. Fresh air in the 21st century. *Geophys. Res. Lett* **2003**, *30*, 72−74.

(3) Stevens, C. J.; N. B. Dise; J. O. Mountford; Gowing, D. J. Impacts of nitrogen deposition on species richness of grassland. *Science* **2004**, *303*, 1876−1879.

(4) Galloway, J. M.; Dentener, F. J.; Capone, D. G.; Boyer, E. W.; Howarth, R. W.; Seitzinger, S. P.; Asner, G. P.; Cleveland, C.; Green, P.; Holland, E.; Karl, D. M.; Michaels, A. F.; Porter, J. H.; Townsend, A.; Charles, V. Nitrogen Cycles: Past, Present and Future. *Biogeochemistry* **2004**, *70*, 153−226.

(5) Dentener, F.; Stevenson, D.; Cofala, J.; Mechler, R.; Amann, M.; Bergamaschi, P.; Raes, F.; Derwent, R. The impact of air pollutant and methane emission controls on tropospheric ozone and radiative forcing: CTM calculations for the period 1990−2030. *Atmos. Chem. Phys.* **2005**, *5*, 1731−1755, SREF-ID: 1680-7324/ap/2005-1735-1731.

(6) Nakicenovic, N.; Alcamo, J.; Davis, G.; De Vries, B.; Fenhann, J.; Gaffin, S.; Gregory, K.; Grübler, A.; Jung, T. Y.; Kram, T.; Lebre La Rovere, E.; Michaelis, L.; Mori, S.; Morita, T.; Pepper, W.; Pitcher, H.; Price, L.; Riahi, K.; Roehrl, A.; Rogner, H. H.; Sankovski, A.; Schlesinger, M.; Priyadarshi Shukla, P.; Steven Smith, S.; Robert Swart, R.; Van Rooijen, S.; Victor, N.; Dadi, Z. Cambridge University Press: Cambridge, United Kingdom and New York, U.S.A., 2000; p 599.

(7) Dentener, F.; Drevet, J.; Stevenson, D. S.; Ellingsen, K.; Van Noije, T.; Schultz, M. g.; Atherton, C.; Bell, N.; Butler, T.; Eickhout, B.; Fiore, A.; Galloway, J. N.; Galy-Lacaux, C.; Kulshestha, U. C.; Lamarque, J. F.; Montanaro, V.; Muller, J.-F.; Rodriguez, J.; Sanderson, M.; Savage, N.; Szopa, S.; Sudo, K.; Wild, O.; Zeng, G. Nitrogen and Sulphur Deposition on regional and global scales: a multi-model evaluation. *Global Biogeochem. Cycles* **2006** in press.

(8) Ellingsen, K.; et; al Ozone air quality in 2030: a multi model assessment of risks for health and vegetation. *J. Geophys. Res.* **2006**, manuscript in preparation.

(9) van Noije, T. P. C.; Eskes, H. J.; Dentener, F. J.; Stevenson, D. S.; Ellingsen, K.; Schultz, M. G.; Wild, O.; Amann, M.; Atherton, C. S.; Bergman, D. J.; Bey, I.; Boersma, K. F.; Butler, T.; Cofala, J.; Drevet, J.; Fiore, A. M.; Gauss, M.; Hauglustaine, D. A.; Horowitz, L. W.; Isaksen, I. S. A.; Krol, M. C.; Lamarque, J.-F.; Lawrence, M. G.; Martin, R. V.; Montanaro, V.; Miller, J.-F.; Pitari, G.; Prather, M. S. E.; Sudo, K.; Szopa, S.; van Roozendael, M. Multi-model ensemble simulations of tropospheric NO2 compared with GOME retrievals for the year 2000. *Atmos. Chem. Phys. Discuss.* **2006**, *6*, 2965−3047.

(10) Stevenson, D. S.; Dentener, F. J.; Schultz, M. G.; Ellingsen, K.; Van Noije, T. P. C.; Wild, O.; Zeng, G.; Amann, M.; Atherton, C. S.; Bell, N.; Bergmann, D. J.; Bey, I.; Butler, T.; Cofala, J.; Collins, W. J.; Derwent, R. G.; Doherty, R. M.; Drevet, J.; Eskes, H. J.; Fiore, A.; Gauss, M. A.; Hauglustaine, D. A.; Horowitz, L. W.; Isaksen, I. S. A.; Krol, M. C.; Lamarque, J. F.; Lawrence, M. G.; Montanero, V.; Müller, J. F.; Pitari, G.; Prather, M. J.; Pyle, J. A.; Rast, S.; Rodriguez, J. M.; Sanderson, M. G.; Savage, N. H.; Shindell, D. T.; Strahan, S. E.; Sudo, K.; Szopa, S. Multi-model ensemble simulations of present-day and near-future tropospheric ozone. *J. Geophys. Res.* **2006**, in press.

(11) Stevenson, D.; Doherty, R.; Sanderson, M.; Johnson, C.; Collins, B.; Derwent, D. Impacts of climate change and variability on tropospheric ozone and its precursors. *Faraday Discuss.* **2005**, *130*, 1−17.

(12) Gauss, M.; Myhre, G.; Pitari, G.; Prather, M. J.; Isaksen, I. S. A.; Berntsen, T. K.; Brasseur, G. P.; Dentener, F. J.; Derwent, R. G.; Hauglustaine, D. A.; L. W. H.; Jacob, D. J.; Johnson, M.; Law, K. S.; Mickley, L. J.; Müller, J.-F.; Plantevin, P.-H.; Pyle, J. A.; Rogers, H. L.; Stevenson, D. S.; Sundet, J. K.; van Weele, M.; Wild, O. Radiative forcing in the 21st century due to ozone changes in the troposphere and the lower stratosphere. *J. Geophys. Res.* **2003**, *108* (D9), 4292, DOI:4210.1029/2002JD002624.

(13) WHO. *Modelling and Assessment of the Summary report*; WHO Task Force on the Health Aspects of Air Pollution of the World Health Organization/European Centre for Environment and Health and the Executive, 2004.

(14) Bobbink, R.; Hornung, M.; Roelofs, J. M. The effects of air-borne pollutants on species diversity in natural and semi-natural European vegetation. *J. Ecol.* **1998**, *86*, 717−738.
(15) Holland, E. A.; Brasswell, B. H.; Lamarque, J. F.; Townsend, A.; Sulzman, J.; Muller, J. F.; Dentener, F.; Brasseur, G.; Levy, H., II; Penner, J. E.; Roelofs, G. J. Variations in the predicted spatial distribution of atmospheric nitrogen deposition and their impact on carbon uptake by terrestial ecosystems. *J. Geophys. Res.* **1997**, *102*, 15849−15866.
(16) Sala, O. E.; Chapin, F. S., III; Armesto, J. J.; Berlow, R.; Bloomfield, J.; Dirzo, R.; Huber-Sanwald, E.; Huenneke, L. F.; Jackson, R. B.; Kinzig, A.; Leemans, R.; Lodge, D.; Mooney, H. A.; Oesterheld, M.; Poff, N. L.; Sykes, M. T.; Walker, B. H.; Walker, M.; Wall, D. H. Global biodiversity scenarios for the year 2100. *Science* **2000**, *87*, 1770−1774.
(17) Fiore, A. M.; Jacob, D. J.; Field, B. D.; D. G. Streets; S. D. Fernandes; Jang, C. Linking ozone pollution and climate change: The case for controlling methane. *Geophys. Res. Lett.* **2002**, *29*, 25−21/25−24, DOI:10.1029/2002GL015601.
(18) West, J. J.; Fiore, A. M. Management of Tropospheric Ozone by Reducing Methane Emissions. *Environ. Sci. Technol.* **2005**, *E39* (13), 4685−4691, DOI:4610.1021/es048629f.
(19) Zunckel, M.; Venjonoka, K.; Pienaar, J. J.; Brunke, E. G.; Pretorius, O.; Koosialee, A.; Raghunandan, A.; Tienhoven, A. M. v. Surface ozone over southern Africa, synthesis of monitoring results during the cross border Air Pollution Impact Assessment project. *Atmos. Environ.* **2004**, *38*, 6139−6147.
(20) Carmichael, G. R.; Ferm, M.; Thongboonchoo, N.; Woo, J.-H.; Chan, L. Y.; Murano, K.; Viet, P. H.; Mossberg, C.; Bala, R.; Boonjawat, J.; Upatum, P.; Mohan, M.; Adhikary, S. P.; Shrestha, A. B.; Pienaar, J. J.; Brunke, E. B.; Chen, T.; Jie, T.; Guoan, D.; Peng, L. C.; Dhiharto, S.; Harjanto, H.; Jose, A. M.; Kimani, W.; Kirouane, A.; Lacaux, J.; Richard, S.; Barturen, O.; Cerda, J. C.; Athayde, A.; Tavares, T.; Cotrina, J. S.; Bilici, E. Measurements of sulfur dioxide, ozone and ammonia concentrations in Asia, Africa, and South America using passive samplers. *Atmos. Environ.* **2003**, *37*, 1293−1308.
(21) Naja, M.; Lal, S. Surface ozone and precursor gases at Gadanki (13.5 N, 79.2 E) a tropical rural site in India. *J. Geophys. Res.* **2002**, *107*, 4179, DOI:4110.1029/2001JD000357.
(22) Naja, M.; Lal, S.; Chand, D. Diurnal and seasonal variabilities in surface ozone at a high altitude site Mt Abu (24.6 N, 72.7 E, 160 ma asl) in India. *Atmos. Environ.* **2003**, *37*, 4205−4215.

Received for review November 28, 2005. Revised manuscript received March 7, 2006. Accepted March 16, 2006.

ES0523845